Butyl rubber as a macro-cross-linker in the preparation of a shape-memory and self-healing polymer

Burak Tavsanli, Cigdem Bilici, Pelin Sungur, et al.

Citation: Journal of Rheology **66**, 1367 (2022); doi: 10.1122/8.0000414
View online: https://doi.org/10.1122/8.0000414
View Table of Contents: https://sor.scitation.org/toc/jor/66/6
Published by the The Society of Rheology

Butyl rubber as a macro-cross-linker in the preparation of a shape-memory and self-healing polymer

Burak Tavsanli,[1] Cigdem Bilici,[2] Pelin Sungur,[2] Semra Ide,[3] and Oguz Okay[1,a)]

[1]*Department of Chemistry, Istanbul Technical University, 34469 Maslak, Istanbul, Turkey*
[2]*Nanotechnology Research and Application Center, Sabanci University, 34956 Tuzla, İstanbul, Turkey*
[3]*Department of Physics Engineering and Department of Nanotechnology and Nanomedicine, Hacettepe University, 06800 Beytepe, Ankara, Turkey*

(Received 10 December 2021; final revision received 6 February 2022; published 1 November 2022)

Abstract

Recently, a simple strategy was developed for preparing interconnected interpenetrating polymer networks (IPNs) based on butyl rubber (IIR) and poly(*n*-octadecyl acrylate) (PC18A). Solvent-free UV polymerization of *n*-octadecyl acrylate (C18A) monomer in the melt of IIR at ambient temperature resulted in IPNs with self-healing and shape-memory functions. Here, we demonstrate that the use of IIR grafted with acrylic acid, methacrylic acid, and 10-undecenoic acid instead of unmodified IIR provides a significant improvement in the mechanical properties of IPNs. Differential scanning calorimetry, small-angle x-ray scattering, and wide-angle x-ray scattering analysis reveal side-by-side packing of C18 side chains of PC18A to form lamellar crystals with a melting temperature T_m between 46 and 52 °C. Transmission electron microscopy analysis indicates the existence of quasispherical nanoparticles composed of crystalline domains, which are dispersed in a continuous interpenetrating rubber-PC18A matrix. This microstructure provides them a complete self-recovery behavior induced by heating and an efficient shape-memory function. IPNs exhibit around tenfold higher chemical cross-link density as compared to those prepared from the native IIR, reflecting the effect of pendant vinyl groups on the extent of covalent interconnections between the IIR and PC18A components. The type of the grafted monomers significantly affects the mechanical performance of IPNs, which can be explained with the individual contributions of chemical and physical cross-links to the total cross-link density. The amount of the grafted rubbers in IPN could be further increased up to 80 wt. % by the incorporation of toluene into the reaction system, resulting in IPNs with a wide range of tunable thermal and mechanical properties. https://doi.org/10.1122/8.0000414

I. INTRODUCTION

Economic recycling of polymer wastes has attracted significant interest for 60 years to reduce the waste amount and the disposal costs. However, a more promising approach that emerged in the past decade is to generate self-healing or self-recoverability in polymeric materials to prolong their service life and hence to reduce the load of waste polymers [1–3]. A large number of studies has been conducted in the past few years to produce self-healing polymers and hydrogels, mainly via intrinsic mechanisms, e.g., by producing them via noncovalent interactions or dynamic covalent bonds. Another important aspect, especially for biomedical applications, is to generate shape-memory in such materials, an ability to memorize one or more shapes under the effect of a stimulus [4]. A prerequisite for shape-memory behavior is the co-existence of at least two types of cross-links with different lifetimes and, hence, bond strengths. Typically, chemical cross-links with infinite lifetime and switchable crystalline domains acting as permanent and temporary cross-links, respectively, are utilized to fabricate shape-memory polymers.

Recently, we presented a simple strategy for preparing self-healing and shape-memory interconnected interpenetrating polymer networks (IPNs) based on butyl rubber (IIR) and poly(*n*-octadecyl acrylate) (PC18A) [5]. IIR, a random copolymer consisting of isobutylene units with 0.5–4 mol. % isoprene unsaturation, is a biocompatible rubber with several attractive properties. The second component of the IPNs, namely, PC18A is a semicrystalline polymer due to its octadecyl (C18) side chains aligning to form lamellar crystals with a melting temperature of around 50 °C. Because IIR is soluble in the monomer *n*-octadecyl acrylate (C18A) above its melting temperature (30 °C), solvent-free UV polymerization of C18A in the presence of IIR results in IPNs with tunable thermal and mechanical properties together with self-healing and shape-memory functions. The number of elastically effective chemical cross-links in IPNs was found to be much lower than the physical cross-links formed by the crystalline domains and hydrophobic associations [5]. This is expected due to the low degree of unsaturation of IIR limiting the cross-linking reactions between its isoprene units and the growing PC18A radicals during the UV polymerization.

In this regard, the chemical modification of IIR to incorporate vinyl groups pendant to the IIR backbone is a particularly attractive strategy since they can easily be cross-linked using free radical initiators via their pendant functionality [6,7]. This is in contrast to the unmodified IIR undergoing extensive chain scission instead of the cross-linking

Note: This paper is part of the special issue on Double Dynamics Polymeric Networks.

[a)]Author to whom correspondence should be addressed; electronic mail: okayo@itu.edu.tr

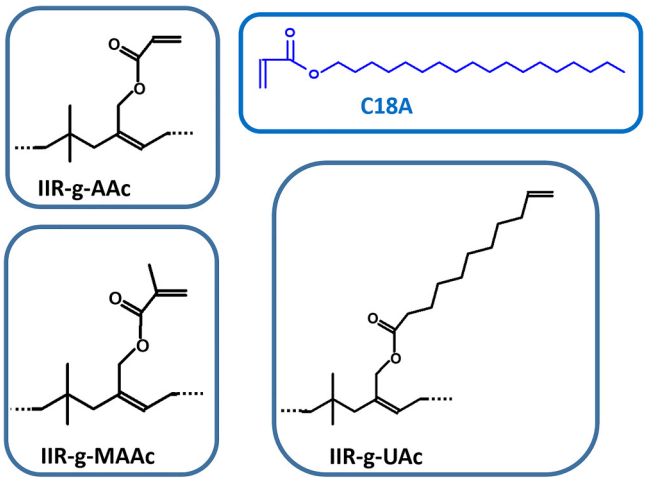

SCHEME 1. Acrylate- and methacrylate-functionalized butyl rubbers (IIR-g-AAc, IIR-g-UAc, and IIR-g-MAAc) and *n*-octadecyl acrylate (C18A) monomer used in the IPN preparation. For the graft rubbers, Z-isomeric form of esters is shown.

reactions. Parent and co-workers prepared a series of IIR macromonomers containing pendant vinyl and styrenic functionalities starting from brominated IIR (BIIR) possessing a significantly higher reactivity as compared to IIR [7]. It was shown that the BIIR-derived macromonomers exhibit a high cross-link efficiently with peroxide initiation to produce high modulus, thermoset products.

The aim of this study was to strengthen the interconnections between IIR rubber and semicrystalline PC18A polymer to produce mechanically strong IPNs without compromising their smart functions. For this purpose, instead of IIR, functionalized IIRs with three different acrylate and methacrylate groups were selected in the IPN preparation, as presented in Scheme 1. These are butyl rubbers bearing acrylic acid (IIR-g-AAc), methacrylic acid (IIR-g-MAAc), and 10-undecenoic acid (IIR-g-UAc) groups, which are abbreviated as grafted IIRs. They were prepared by transforming the bromine functionality of BIIR into pendant acrylate or methacrylate groups as described by Parent *et al.* [6,7]. After dissolving the grafted IIRs in the melt of C18A containing Irgacure photoinitiator, the photopolymerization at ambient temperature results in mechanically robust IPNs consisting of 20–40 wt. % grafted IIRs with shape-memory and self-healing behavior. The amount of the grafted rubbers in IPN could be further increased up to 80 wt. % by the incorporation of toluene, a good solvent for both rubber and C18A, into the reaction system resulting in IPNs with a wide range of tunable thermal and mechanical properties.

II. EXPERIMENTAL

A. Materials

Bromobutyl rubber (BIIR, Bromobutyl X2, Lanxess Int) was purified by dissolving in toluene and precipitating in methanol followed by drying under vacuum to constant mass. *n*-Octadecyl acrylate (C18A), acrylic acid (AAc), methacrylic acid (MAAc), 10-undecenoic acid (UAc), 2-hydroxy-4′-(2-hydroxyethoxy)-2-methylpropiophenone (Irgacure 2959), tetrabutylammonium hydroxide (Bu_4NOH), and tetrabutylammonium bromide (Bu_4NBr) were obtained from Sigma-Aldrich (St. Louis, MO) and used as received.

B. Synthesis of grafted IIRs

They were prepared as described by Parent *et al.* and detailed in the text given in the supplementary material [6,7,21]. Briefly, to prepare IIR-g-AAc, AAc (0.21 g, 3 mmol) was dissolved in 3 ml of methanolic 1M Bu_4NOH (3 mmol) under stirring to obtain tetrabutylammonium salt of acrylic acid (AAc^- Bu_4N^+) that was isolated by the evaporating methanol under vacuum. AAc^- Bu_4N^+ (0.94 g, 3 mmol) was then added into 100 g of toluene containing BIIR (10 g) and Bu_4NBr (0.48 g, 1.5 mmol). After stirring the solution at room temperature for 1 h, and at 85 °C for 3 h, the esterification product IIR-g-AAc was purified by reprecipitation from *n*-hexane solution in acetone twice and finally drying under vacuum. IIR-g-AAc was obtained with a quantitative yield.

C. Preparation of IPNs

UV polymerization of C18A was conducted in the presence of the grafted IIRs and Irgacure 2959 photoinitiator at 360 nm. The rubber content in the melt mixture was changed from 20 to 40 wt. %. For instance, to prepare an IPN containing 20 wt. % IIR-g-UAc, IIR-g-UAc (1.0 g) was dissolved in C18A (4.0 g) under stirring at 80 °C for 24 h to produce a transparent mixture. Irgacure 2959 (8 mg, 0.2 wt. % of C18A) was then added and stirred for 5 min. The mixture was then transferred to a glass mold sized $5 \times 5 \times 1$ mm^3, and the photopolymerization was conducted at 30 ± 2 °C for 1.5 h under UV light at 360 nm. For the preparation of IPNs in the presence of toluene, the same procedure was used except that toluene (4 ml) was included into the melt mixture to obtain a rubber +C18A solution at a concentration of 59 wt. %. IPNs, thus, formed in toluene were dried under vacuum to constant mass.

D. Characterization

The molecular structures of the starting rubber BIIR and grafted IIRs were determined by ^1H nuclear magnetic resonance (^1H NMR, Agilent VNMRS 500 MHz) using $CDCl_3$ as the solvent as detailed in the text, Figs. S1 and S2, and Tables S1 and S2 in the supplementary material [21]. Their molecular weights were measured by gel permeation chromatography (GPC) on a Malvern GPC max instrument (RI detector, mobile phase: THF) using polystyrene standards (PolyCal, Malvern). A Perkin Elmer Diamond differential scanning calorimeter (DSC) was used to evaluate thermal transitions of IPNs under constant nitrogen purge. The samples in hermetic pans were heated from 5 to 80 °C at a heating rate of 5 °C min^{-1} and then cooled back to 5 °C at the same rate. The degree of crystallinity f_{cry}, i.e., the fraction of C18A units forming alkyl crystals was determined by dividing the melting enthalpy of the samples with the enthalpy of 100% crystalline PC18A [5]. Wide-angle (WAXS) and small-angle x-ray scattering (SAXS) experiments of IPNs were performed on a HECUS-SWAXS system (Graz, Austria) using a

nickel filtered CuK$_\alpha$ radiation source ($\lambda = 0.154$ nm), operating at 50 kV/40 mA. While the shape, size, and distance distributions of the nanoaggregations were determined by the SAXS method, it was also investigated whether there was a change in the crystalline arrangements of the nanoformations with the simultaneous WAXS analysis. The morphology of IPNs stained with UranyLess was evaluated by transmission (TEM) and scanning transmission electron microscopy (STEM) on a JEOL ARM-200CF instrument operating at 200 kV, as detailed before [5]. Quantitative analysis of the dispersed crystalline nanoparticles in IPNs was conducted from the TEM micrographs using the IMAGEJ software (NIH, USA). The area of at least individual 100 particles was measured, from which sphere-equivalent diameters were calculated [5].

The viscoelasticity of IPN samples (diameter 20 mm, thickness ~1 mm) was investigated using oscillatory shear rheology tests conducted on a Bohlin Gemini 150 rheometer (Malvern) with a parallel plate geometry (diameter 20 mm) equipped with Peltier-temperature controller system. Frequency sweep was carried out from 0.4 to 100 rad s^{-1} at a strain amplitude of 0.1% in the linear viscoelastic region. The tensile properties were measured at 23 ± 2 °C by using a Zwick Roell testing machine equipped with a 500 N load cell at a constant crosshead rate of 5 min^{-1}. Rectangular samples with length = 30 mm, width = 20 mm, thickness = 1 mm, and a gauge length of 10 mm were used. Young's modulus E was calculated from the linear region of the stress-strain curve, as the slope between 0.01% and 2% strain, while the toughness (work of extension) W was calculated by the area under the stress-strain curve. Cyclic tests were conducted as above by successive loading and unloading the samples without a waiting time between cycles. The dissipated (hysteresis) energy U_{hys} was estimated by the area within the cycle, and the fraction of dissipated energy f_{diss} is defined as the U_{hys} relative to the area under the loading curve.

The self-healing performance of IPNs was investigated by the cut-and-heal test conducted on specimens of dimensions $2 \times 1 \times 1$ mm^3. They were cut using a razor blade and the interfaces were repositioned together. After healing at 65 °C for 24 h followed by cooling to room temperature, their mechanical properties were measured using the Zwick Roell testing machine as detailed above. For the shape-memory testing, the samples of the same size as above were immersed in a water bath at 65 °C for 5 min, deformed to an U-shape, and then immersed in a water bath at 15 °C for 5 min. The shape recovery was started by heating the specimen in a water bath from 15 to 85 °C during which the deformation angle θ_d is measured by IMAGEJ software [5]. The shape-recovery ratio R_θ was estimated as $R_\theta = \theta_d/180$. The equilibrium weight swelling ratio q_w and soluble fraction w_{sol} of IPN specimens were conducted in toluene as described elsewhere [5].

III. RESULTS AND DISCUSSIONS

IPNs were prepared by first dissolving grafted IIRs in C18A to obtain a homogeneous solution. After the addition of Irgacure initiator, solvent-free UV photopolymerization of C18A was conducted at 30 ± 2 °C for 1.5 h. The extraction of the resulting IPNs in toluene leads to a soluble fraction w_{sol} of less than 3 wt. % revealing the occurrence of the chemical cross-linking reactions between their components (Table S3 in the supplementary material [21]). The rubber content of IPNs could be increased up to 40 wt. % due to the high viscosity of the melt mixture. However, addition of toluene in the reaction system provides formation of IPNs with a rubber content of up to 80 wt. %. In the following, we first discuss the properties of the grafted IIRs used as the starting material for IPNs. Microstructure of IPNs and their viscoelastic, mechanical, self-healing, and shape memory properties were discussed in Secs. III A–III D. The effect of toluene addition at the preparation stage on the properties of IPNs was then presented in Sec. III E.

A. Grafted IIRs

Bromobutyl rubber (BIIR) containing 0.84 mol. % bromine, as determined by ^{1}H-NMR, was functionalized using acrylic acid (AAc), methacrylic acid (MAAc), and 10-undecenoic acid (UAc) to obtain grafted butyl rubbers denoted as IIR-g-AAc, IIR-g-MAAc, and IIR-g-UAc, respectively (Scheme 1). Table I shows the characteristics of the starting rubber BIIR, and grafted IIRs including the amount of pendant vinyl groups, the fraction of the isomeric forms, the number-average molecular weights, and the polydispersity indices. BIIR is known to exist in two isomeric forms, namely, the exo-methylene allyl bromide (Exo) and endo-bromomethyl olefin [8]. BIIR used in this study has 88% exo-isomer, the rest being endo Z- and E-esters (Table I, Figs. S1and S2 in the supplementary material [21]). After its esterification with AAc, MAAc, and UAc monomers, the resulting grafted rubbers carrying pendant vinyl groups have predominantly Z-ester isomer, as reported before (Table I) [7]. Moreover, the molecular weight of BIIR slightly decreases after its functionalization, which is attributed to the decrease of its hydrophobicity and, hence, the change in the hydrodynamic radius. Table I also shows that the grafted rubbers have 0.58–0.68 mol. % pendant vinyl groups. Because BIIR contains 0.84 mol. % allylic bromine, which is the upper limit for the degree of acrylation or methacrylation, this means a grafting efficiency of 70%–80%. Calculations using the molecular weight of the grafted rubbers reveal that the average number of vinyl groups pendant to a grafted IIR

TABLE I. The characteristics of BIIR and grafted IIRs including the amount of pendant vinyl groups, the fraction of the isomeric forms ($f_{exo\text{-}ester}$, $f_{E\text{-}ester}$, $f_{Z\text{-}ester}$), the number-average molecular weights ($\overline{M_n}$), and polydispersity indices (PDI). Details are given in the text, Tables S1 and S2, and Figs. S1 and S2 in the supplementary material [21].

Rubber	Pendant vinyl %	$f_{exo\text{-}ester}$	$f_{E\text{-}ester}$	$f_{Z\text{-}ester}$	$\overline{M_n}$ (kg mol^{-1})	PDI
IIR-g-AAc	0.58	0.27	0.21	0.52	220	4.7
IIR-g-MAAc	0.68	0.38	0.15	0.47	270	1.7
IIR-g-UAc	0.68	0.43	0.08	0.49	280	2.9
BIIR	0	0.88	0.12		330	2.7

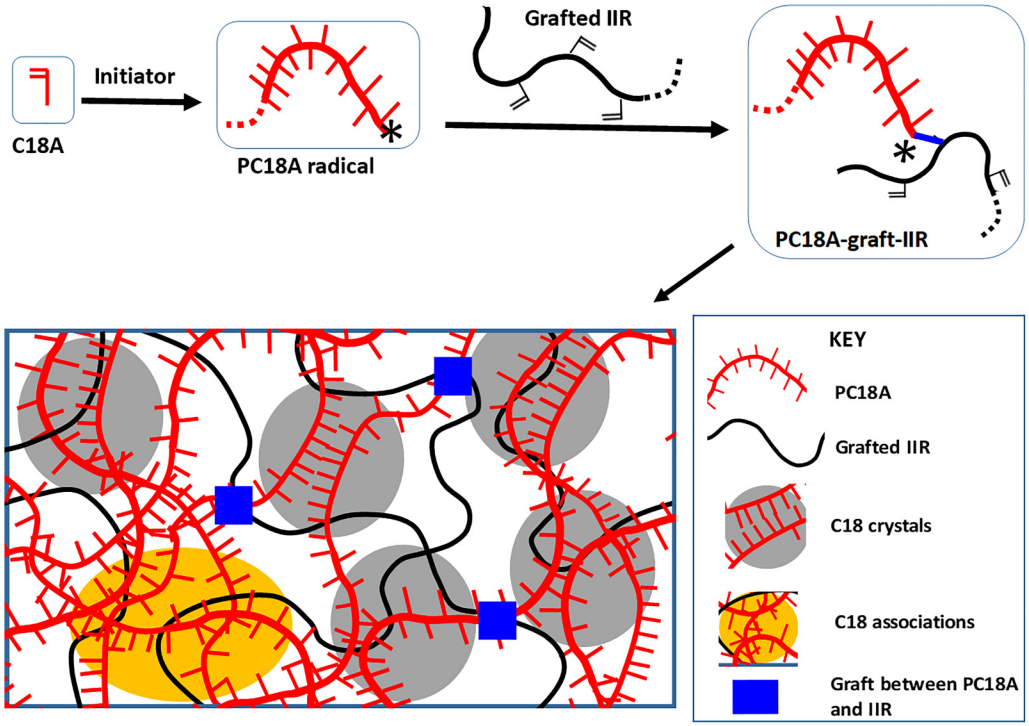

SCHEME 2. Cartoon showing the formation of IPNs by *in situ* polymerization of C18A in the melt of IIR bearing pendant vinyl groups.

chain is between 23 and 34. Thus, the esterification reactions convert BIIR into a multifunctional IIR-based macro-cross-linker able to create chemical cross-links with the growing PC18A radicals during the IPN formation (Scheme 2).

B. Thermal properties, microstructure, and morphology of IPNs

DSC scans of IPNs formed from IIR-g-AAc, IIR-g-UAc, and IIR-g-MAAc rubbers at various amounts are shown in Fig. 1(a). In contrast to the starting BIIR exhibiting no peak in the DSC scans (not shown), all IPNs exhibit melting and crystallization peaks at around 50 and 38 °C, respectively. Figures 1(b) and 1(c) present the melting T_m and crystallization temperatures T_{cry}, and the crystallinity degree f_{cry} of IPNs plotted against the grafted IIR content. Both T_m and T_{cry} slightly decrease by changing the type of the grafted monomers in the order of UAc > AAc > MAAc. Thus, the highest transition temperature is reached using IIR-g-UAc, which is attributed to the long alkyl side chain of UAc stabilizing crystalline octadecyl (C18) side chains of PC18A. Moreover, α-methyl groups of MAAc units are known to hinder the alignment of PC18A backbone leading to weaker crystals with a lower T_m and T_{cry} [9]. The degree of the crystallinity f_{cry} that is close to 50% for pure PC18A decreases with increasing IIR content due to the steric hindrance of the grafted rubbers.

The crystalline structures and nano-scaled structural changes of IPNs were simultaneously investigated by SAXS and WAXS measurements. Figures 2(a) and 2(b) show SAXS and WAXS patterns, respectively, for IPN's containing 20 wt. % grafted rubbers, where the scattering intensity I (q) is plotted against the magnitude of scattering vector q (a) and scattering angle 2θ (b). SAXS data reveal a broad peak for all IPNs at around 0.1 $Å^{-1}$ corresponding to a long spacing d_2 of ~6.3 nm. This peak typically corresponds to the backbone-to-backbone distance of PC18A segments in the lamellar crystals [9–13]. However, it is much broader than that of semicrystalline PC18A, suggesting that the alkyl

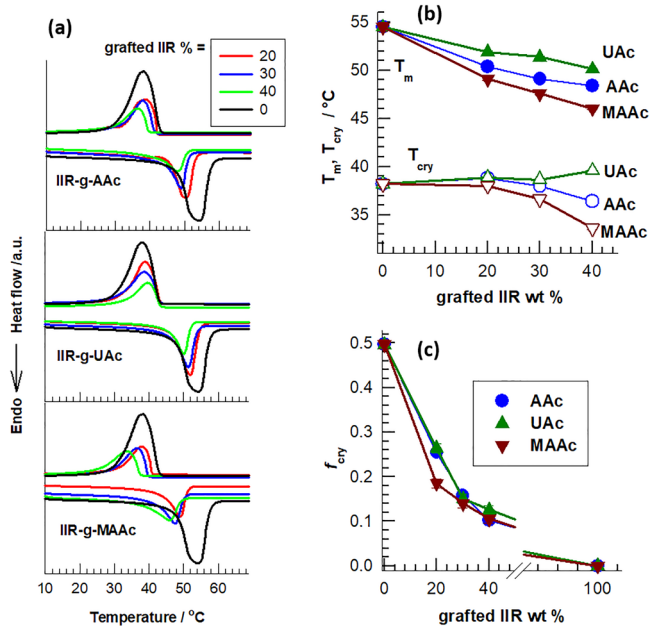

FIG. 1. (a) DSC scans of IPNs formed from IIR-g-AAc, IIR-g-UA, and IIR-g-MAAc at various amounts as indicated. (b) and (c) The melting T_m and crystallization temperature T_{cry} (b) and the degree of crystallinity f_{cry} (c) plotted against the grafted IIR content. The type of the grafted monomers is indicated.

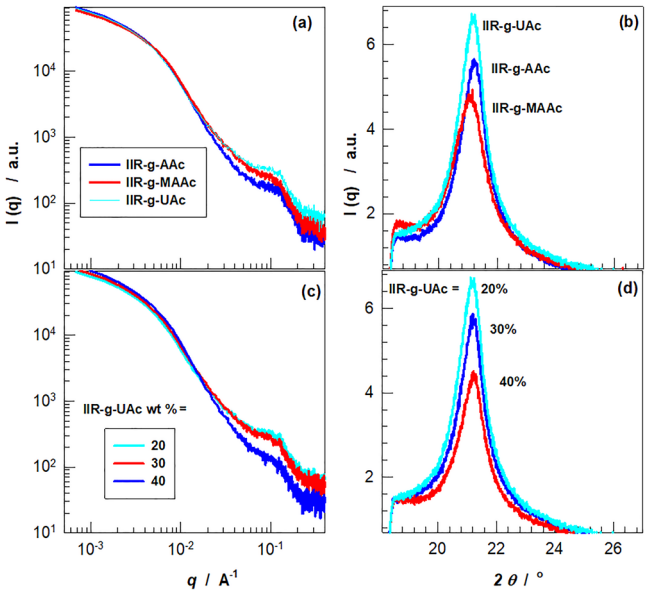

FIG. 2. (a) and (b) SAXS (a) and WAXS patterns (b) of IPNs formed using 20 wt. % IIR grafted with UAc, AAc, and AAc, as indicated. (c) and (d) SAXS (c) and WAXS patterns (d) of IPNs formed using IIR-g-UAc with different amounts as indicated.

crystals are not well-ordered, likely due to the steric effect of the rubber component of IPN. WAXS data show a common sharp peak at 21.2°, which is typical for short-range ordering of C18 side chains with a d_1 spacing of 0.42 nm [9,10,11,14,15]. In accord with the DSC results, the intensity of both SAXS and WAXS peaks is highest for the IPN containing IIR-g-UAc rubber, revealing that UAc facilitates side-by-side packing of C18A side chains. Figures 2(c) and 2(d) present SAXS and WAXS data, respectively, for IPNs formed using 20–40 wt. % IIR-g-UAc as indicated. Although the position of the peaks is independent of the rubber content, their intensity decreases as the rubber content is increased indicating formation of less ordered weaker crystals. From these results, we conclude that the incorporation of UAc side chains in the rubber produces the most stable crystals in IPNs while their degree of crystallinity f_{cry} is almost independent of the type of the grafted monomer.

Figures 3(a)–3(c) show TEM images in the bright-field (BF) mode for IPNs prepared using 20 (a), 30 (b), and 40 wt. % IIR-g-UAc. The scale bars are 1 μm and 500 nm in the upper and bottom panels, respectively. Low magnification images covering a larger area for IPNs are given in Figs. S3 in the supplementary material [21]. The specimens were stained with UranyLess and, hence, the crystalline and amorphous areas appear dark and bright, respectively [5]. IPNs consist of quasispherical semicrystalline nanoparticles distributed in an amorphous matrix. The size distribution of the nanoparticles was estimated from measurements of at least 100 particles from images of different magnifications and compiled in Fig. 3(d). The average diameter decreases from 494 ± 105 to 113 ± 25 nm, and the size distribution becomes narrower as the rubber content is increased from 20 to 40 wt. %. The inverse relation between the diameter of the nanoparticles and the rubber content is attributed to the increase in the viscosity of the melt mixture with increasing rubber content hindering the agglomeration between the nanoparticles during the polymerization. TEM analysis of IPNs prepared at 20 wt. % IIR-g-UAc, IIR-g-MAAc, and IIR-g-AAc revealed that the particle diameter remains constant at around 0.5 μm independent of the type of the grafted rubber (Fig. S3 in the supplementary material [21]). Figure 4 and Fig. S4 in the supplementary material [21] show dark-field (DF) STEM images of the IPN specimens and their energy-dispersive x-ray spectroscopy (EDX) maps for the carbon C (red, bottom right), oxygen O (green, bottom left), and overlapping signals of C and O atoms (yellow, top right). The bright areas in DF STEM images indicate the crystalline nanoparticles in IPNs. Considering that the oxygen contents of PC18A and the grafted rubbers are 9.9 and 0.1 at. %, respectively, the elemental maps of O atoms indicate the distribution of PC18A over the whole investigated area, i.e., both in and out of the nanoparticles. The single-point STEM-EDX analysis over the STEM micrographs shown in the figures revealed that the O content within the particles is higher than that in the continuous amorphous phase reflecting localization of PC18A chains in the nanoparticles, although they also distribute over the whole area. Thus, the morphology of IPNs consists of nano-sized crystalline domains, which are dispersed in an interconnected amorphous IPN matrix composed of noncrystalline PC18A and rubber components (Scheme 2).

C. Viscoelastic and mechanical properties

The existence of crystalline domains in IPNs was also reflected by the drastic change in their storage modulus G' between below and above T_m. Figures 5(a) and 5(b) show the angular frequency (ω) dependences of G' and the loss factor tan δ of IPNs containing 20–40 wt. % IIR-g-UAc at 25 (a) and 65 °C (b), i.e., at below and above T_m. The extent of the modulus variation with temperature increases with decreasing amount of the rubber and becomes 3 orders of magnitude at 20 wt. % IIR-g-UAc (between 12 MPa and 13 kPa at $\omega = 6.3$ rad s^{-1}). The change in the modulus depending on temperature is completely reversible, similar to the IPNs prepared from unmodified IIR [5]. Moreover, G' vs ω plots of IPNs follow a power law behavior with exponents 0.01 ± 0.01 and 0.08 ± 0.01 at 25 and 65 °C, respectively, indicating increasing frequency dependence of the modulus above T_m. Simultaneously, tan δ increases from below to above 0.1 by heating above T_m revealing a more viscous character of the IPN under sinusoidal strain.

Figures 6(a) and 6(b) show uniaxial tensile stress-strain curves at 23 ± 2 °C for IPNs containing 20 and 40 wt. % grafted IIRs, respectively. For comparison, the curves for IPNs prepared from unmodified IIR are also shown in the figures by the gray curves. The mechanical parameters of IPNs are compiled in Fig. 6(c), where Young's modulus E, fracture stress σ_f, fracture strain ϵ_f, and toughness W (the work of extension) are plotted against the rubber content. The stress-strain curves reveal a significant increase in the fracture stress of IPNs by replacing the native IIR with the grafted one. Young's modulus E of the present IPNs varies

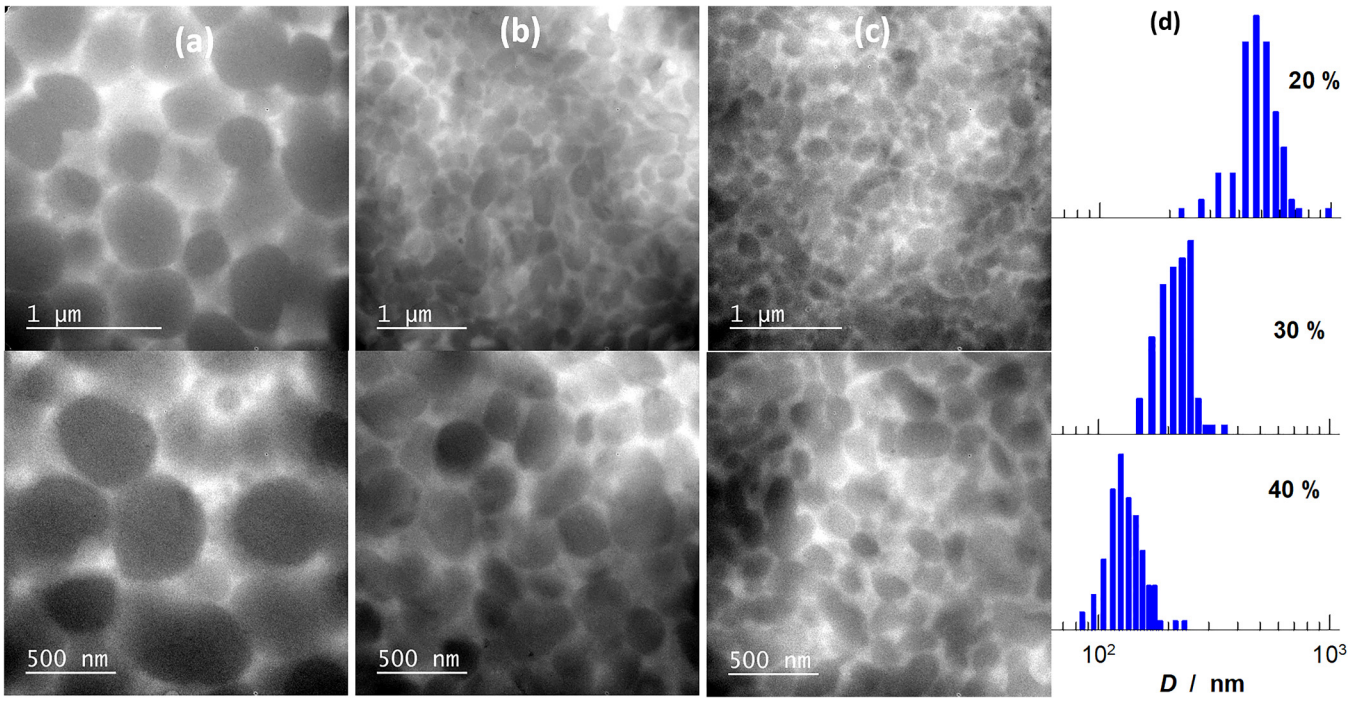

FIG. 3. (a)–(c) TEM images in the BF mode for IPNs prepared using 20 (a), 30 (b), and 40 wt. % (c) IIR-g-UAc. The scale bars are 1 μm and 500 nm in the upper and bottom panels, respectively. (d) The size distribution of the nanoparticles in IPNs formed using 20, 30, and 40 wt. % IIR-g-UAc (from up to down).

between 15 and 120 MPa as compared to 7–34 MPa for IPNs from native IIR. Thus, a significant improvement in the mechanical properties is observed by utilization of acrylate or methacrylate grafted IIRs in the IPN preparation. Moreover, when comparing the effect of the type of grafted monomers on the mechanical performance of IPNs, the highest modulus and fracture stress are obtained using AAc-functionalized IIR while MAAc functionalization produces the highest stretchability and toughness but relatively low modulus. Thus, the mechanical properties of IPNs can be tuned not only by the amount of the grafted rubber but also by the type of the grafted monomer.

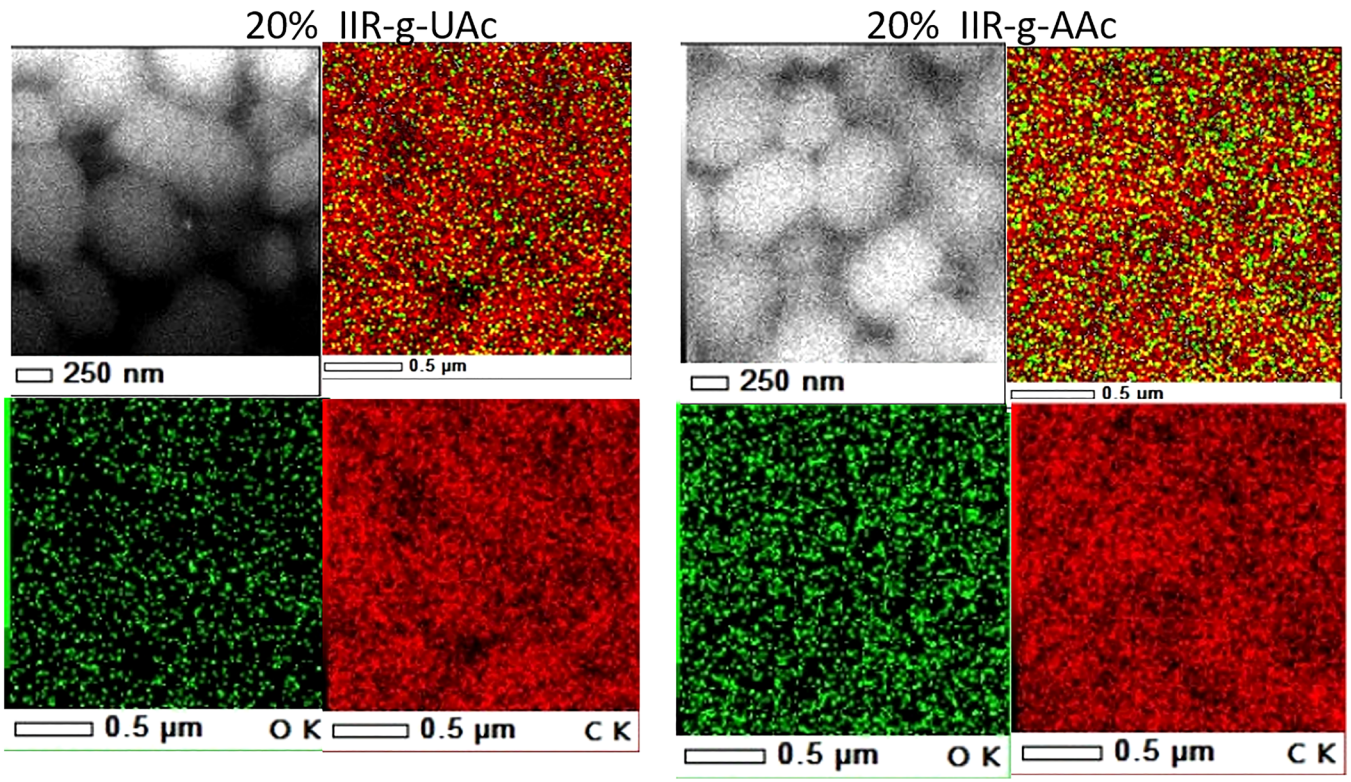

FIG. 4. DF STEM images of IPNs prepared using IIR-g-UAc (left) and IIR-g-UAc (right), each 20 wt. %, and their EDX maps.

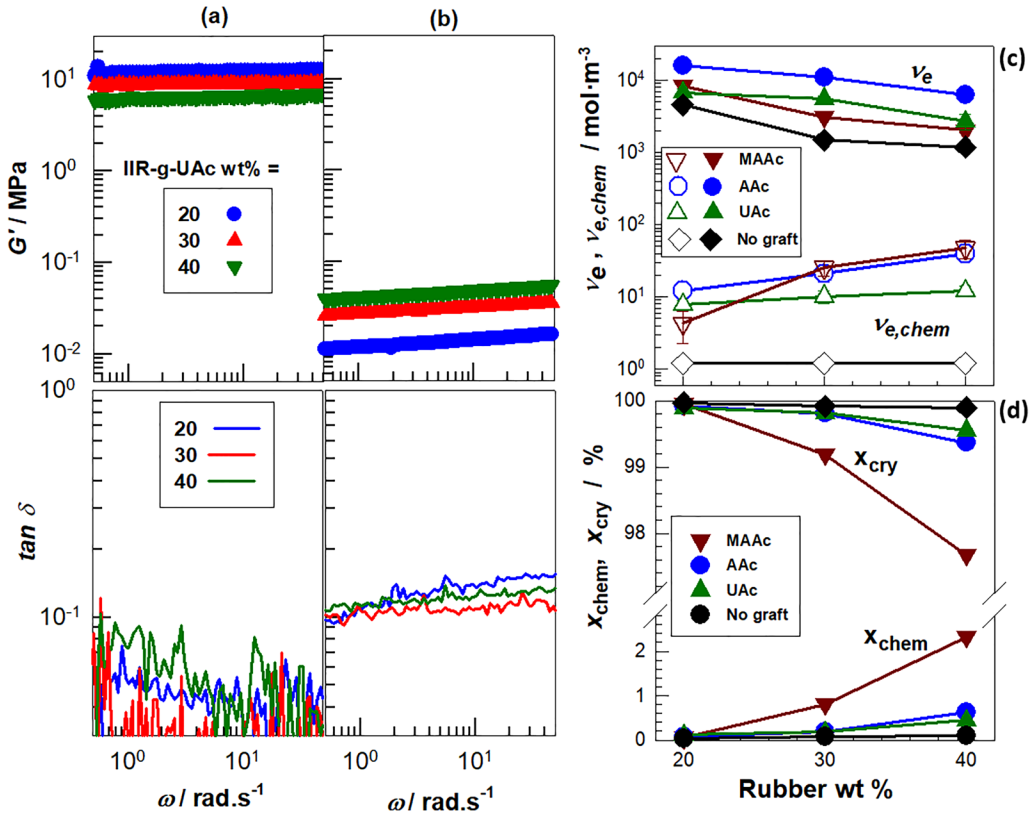

FIG. 5. (a) and (b) Frequency (ω) sweep of G' and tan δ for IPNs containing IIR-g-UAc at 25 (a) and 65 °C (b). $\gamma_o = 0.1\%$. (c) The chemical $\upsilon_{e,\mathrm{chem}}$ (open symbols) and the total cross-link densities υ_e (filled symbols) of IPNs plotted against the rubber content. The types of rubbers are IIR-g-AAc (circles), IIR-g-UAc (triangles up), IIR-g-MAAc (triangles down), and native IIR (diamonds). (d) The contributions of the chemical cross-links x_{chem}, and crystalline domains including hydrophobic associations, x_{cry} to the total cross-link density of IPNs, both plotted against the rubber content. The explanations for the symbols are the same as in (c).

To understand why the type of the grafted monomer affects the mechanical properties of IPNs, we calculated the relative contributions of chemical and physical cross-links to their total cross-link density. Because both the alkyl crystals and hydrophobic associations in semicrystalline polymers or hydrogels disappear upon swelling in good solvents [11–13,16], the elastically effective chemical cross-link density $\upsilon_{e,\mathrm{chem}}$ of IPNs was estimated from their equilibrium weight swelling ratios q_w in toluene (Table S3 in the supplementary material [21]), combined with the Flory–Rehner

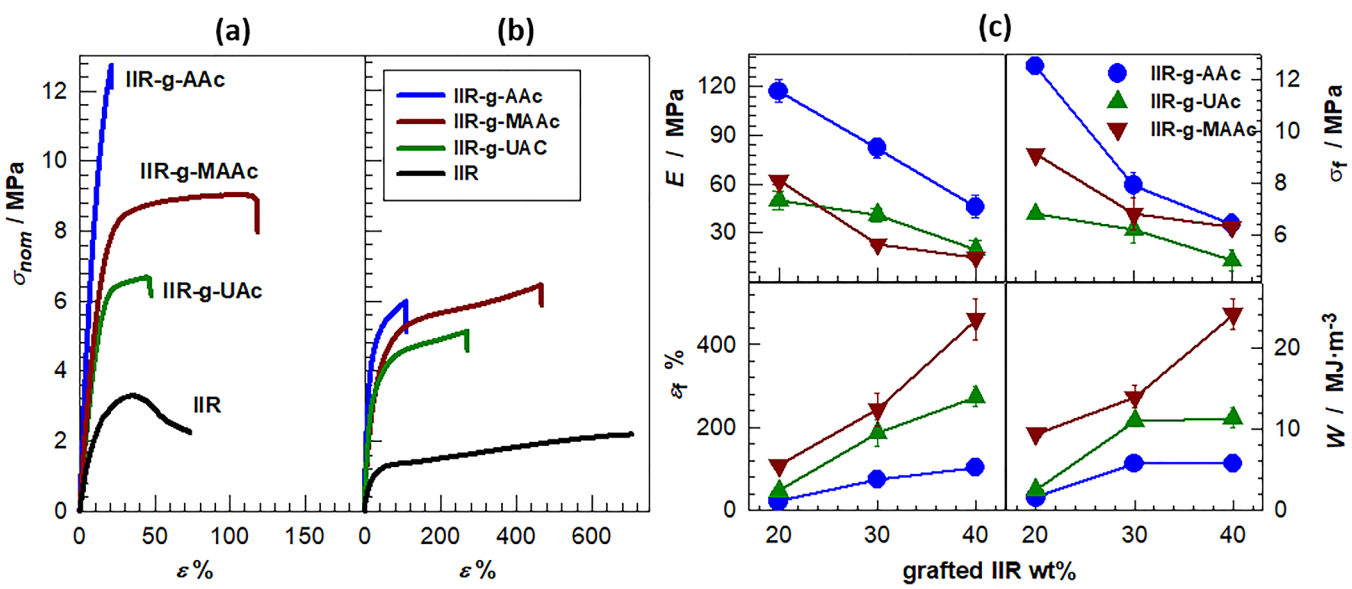

FIG. 6. (a) and (b) Tensile stress-strain curves of IPNs containing 20 (a) and 40 wt. % grafted IIRs (b). The curves for IPNs prepared from unmodified IIR are also shown by the gray curves. (c) Young's modulus E, fracture stress σ_f, fracture strain ϵ_f, and toughness W of IPNs plotted against the rubber content.

equation [17],

$$\upsilon_{e,\text{chem}} = \frac{-[\ln(1-\phi_2) + \phi_2 + \chi(\phi_2)^2]}{V_1[\phi_2^{1/3} - \phi_2/2]}, \quad (1)$$

where ϕ_2 is the volume fraction of cross-linked IPN in the equilibrium swollen state, i.e., $\phi_2 = d_1/(\rho\, q_w)$, χ is the concentration dependent Flory chi parameter taken as $\chi = 0.49 + 0.25\,\phi_2$ (solution cross-linked IIR/toluene system) [18], ρ is the density of IPN (0.92 g ml^{-1}), and d_1 and V_1 are the density and molar volume of toluene 0.867 g ml^{-1} and 106 ml mol^{-1}, respectively. Moreover, assuming a Poisson ratio of 0.5, i.e., $E = 3G$, where G is the shear modulus, the total cross-link density υ_e due to the chemical cross-links, crystalline domains and hydrophobic associations were calculated by $\upsilon_e = E/(3RT)$ [19,20], where R is the gas constant and T is the absolute temperature (296 K). We should note that the IPNs also contain entanglements that may affect their total cross-link density above T_m where only hydrophobic associations and chemical cross-links are effective in forming the 3D network structure.

The open and filled symbols in Fig. 5(c) show the chemical $\upsilon_{e,\text{chem}}$ and total cross-link densities υ_e of IPNs, respectively, prepared from both grafted and native IIR plotted against the rubber content. Several interesting features can be seen when comparing the calculation results with the mechanical parameters of IPNs (Fig. 6). All IPNs produced from grafted IIR exhibit around tenfold higher chemical cross-link density $\upsilon_{e,\text{chem}}$ as compared to those formed from the native IIR, reflecting the effect of pendant vinyl groups on the extent of covalent interconnections between the IIR and PC18A components. The lowest $\upsilon_{e,\text{chem}}$ was observed for the IPN prepared using IIR-g-UAc, which is attributed to the steric hindrance exerted by UAc side chains to the cross-linking reactions. Moreover, both the chemical $\upsilon_{e,\text{chem}}$ and total cross-link densities υ_e are highest for the IPN derived from AAc-functionalized IIR. As a consequence, the highest modulus and fracture stress were obtained using IIR-g-AAc rubber. It is also noteworthy to mention that the incorporation of α-methyl group into IIR-g-AAc to produce IIR-g-MAAc significantly changes the IPN properties [Fig. 6(c)]. To highlight this effect, the individual contributions of the chemical cross-links (x_{chem}) and crystalline domains including hydrophobic associations (x_{cry}) to the total cross-link density (υ_e) of IPNs were calculated using $x_{\text{chem}} = \upsilon_{e,\text{chem}}/\upsilon_e$ and $x_{\text{cry}} = 1 - x_{\text{chem}}$, respectively, and plotted against the rubber content in Fig. 5(d). It is seen that x_{chem} is highest while x_{cry} is lowest for IPNs produced from IIR-g-MAAc due to their relatively low T_m and T_c temperatures [Fig. 1(b)] and the existence of less ordered alkyl crystals [Fig. 2(b)]. These changes in the IPN structure due to the methacrylated IIR result in the highest stretchability and toughness over all IPNs.

D. Self-healing and shape-memory functions

Cyclic mechanical tests were conducted by successive stretching and relaxing of IPN specimens up to a maximum elongation ratio of 70% without a waiting time between cycles. All IPNs subjected to five-successive loading-unloading cycles exhibited irreversible deformation, indicating formation of microcracks before a macroscopic failure (Fig. S5 in the supplementary material [21]). This behavior is also presented in Fig. 7(a) for an IPN specimen with 30 wt. % IIR-g-UAc subjected to two-successive tensile cycles, where the loading and unloading curves are shown by the solid and dashed curves. The hysteresis energy U_{hys} and the modulus E decrease from 2.5 ± 0.2 to 1.0 ± 0.1 MJ m^{-3} and from 37 ± 3 to 1.4 ± 0.1 MPa, respectively, after the first cycle revealing occurrence of a significant microscopic damage in the sample [Fig. 7(b)]. However, when the damaged sample after the first cycle is heated to 65 °C for 10 min and then cooled to the room temperature (23 ± 2 °C), the second loading follows the first one reflecting a complete recovery of the virgin microstructure, as seen by the U_{hys} and E values in Fig. 7(b). Although all IPNs exhibited a complete self-recovery behavior induced by heating, cut-and-heal tests revealed that they have a low self-healing efficiency with respect to their ultimate mechanical properties. The tests were carried out by bringing the cut surfaces of the samples together and heating at 65 °C for 24 h followed by cooling to room temperature. Figure 7(c) shows stress-strain curves of virgin (solid curves) and healed IPNs (dashed curves) with various contents of IIR grafted with AAc, UAc, and MAAc. The healing efficiency with respect to the modulus E is almost complete, e.g., the average efficiency for all IPNs is 95 ± 2%. However, the efficiency with respect to fracture stress and fracture strain remains at a low level, i.e., 30–70% and 3–40%, respectively (Fig. S6 in the supplementary material [21]). This low healing efficiency as compared to the IPN prepared from unmodified IIR is attributed to the increase in the chemical cross-link density of the grafted IIR system relative to the unmodified IIR system [Fig. 5(c)]. Moreover, IPNs containing IIR-g-MAAc exhibit the lowest healing efficiency among others. This is due to the highest percentage of the chemical cross-links in IPNs formed from IIR-g-MAAc as compared to other IPNs. As seen in Fig. 5(d), the individual contribution of the chemical cross-links to the total cross-link density, denoted by x_{chem}, is 2.3%, 0.6%, and 0.4% for IPNs with 40 wt. % MAAc-, AAc-, and UAc-grafted IIRs, respectively.

In contrast to the low healing efficiency of IPNs as compared to those derived from native IIR, they all exhibited an effective shape-fixity and shape-recovery behavior as demonstrated by the bending tests. The specimens in the permanent rod shape are deformed at $T > T_m$ to an U-shape, and this temporary shape is fixed by cooling below T_m prior to the measurements. Figure 8(a) shows the recovery efficiency of the permanent shape in terms of the shape-recovery ratio R_θ of IPNs plotted against the temperature. The deformed U-shape of the specimens remains almost unchanged up to 48 ± 1 °C, i.e., shape-fixity ratio is complete until the vicinity of the melting temperature. The recovery of the permanent shape immediately starts above this temperature, and the shape-recovery ratio R_θ increases from 0 to 94% with 1 °C rise in temperature. The rate of the shape-recovery dR_θ/dT with temperature shows a peak at 49 ± 1 °C for IPNs prepared from all grafted rubbers [Fig. 8(b)].

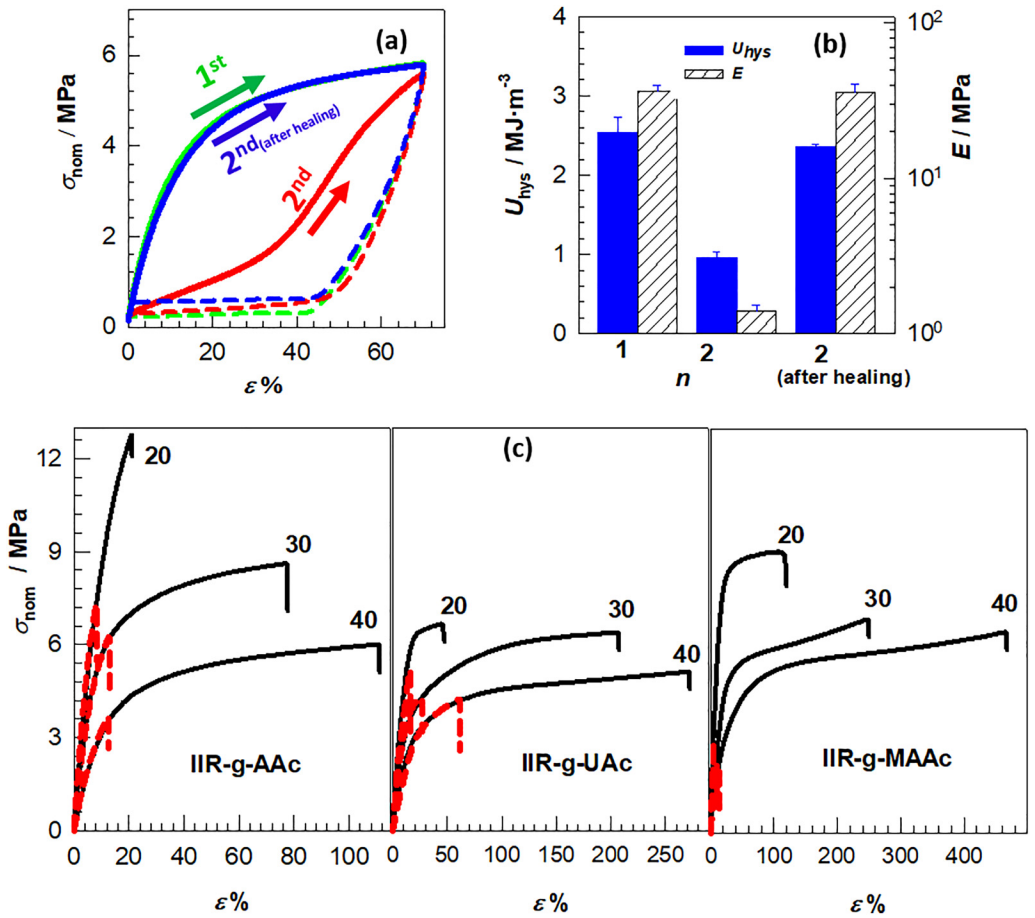

FIG. 7. (a) Cyclic tensile stress-strain curves for an IPN specimen with 30 wt. % IIR-g-UAc. The loading and unloading curves are shown by the solid and dashed curves. (b) The hysteresis energy U_{hys} and the modulus E of the specimen shown as a function of the cycle number n. (c) Stress-strain curves of virgin (solid curves) and healed IPNs (dashed curves). The type and amount of the grafted rubbers are indicated.

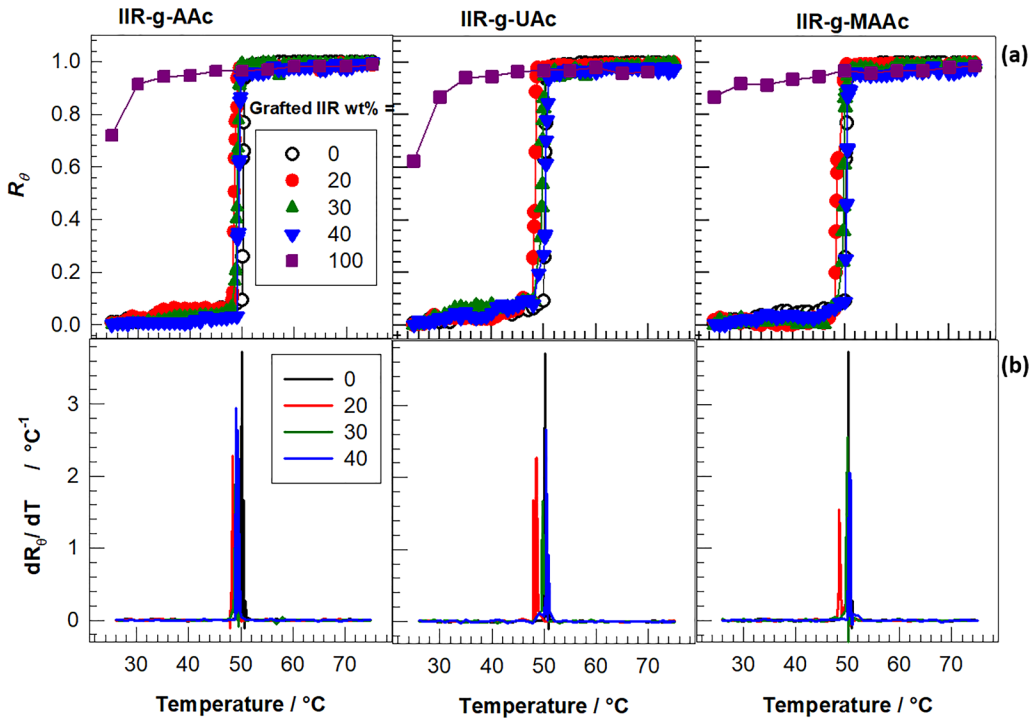

FIG. 8. (a) The shape-recovery ratio R_θ of IPNs plotted against the temperature. The types of grafted rubbers are indicated. (b) The rate of the shape-recovery dR_θ/dT plotted against the temperature. The colors correspond to the symbol colors in (a).

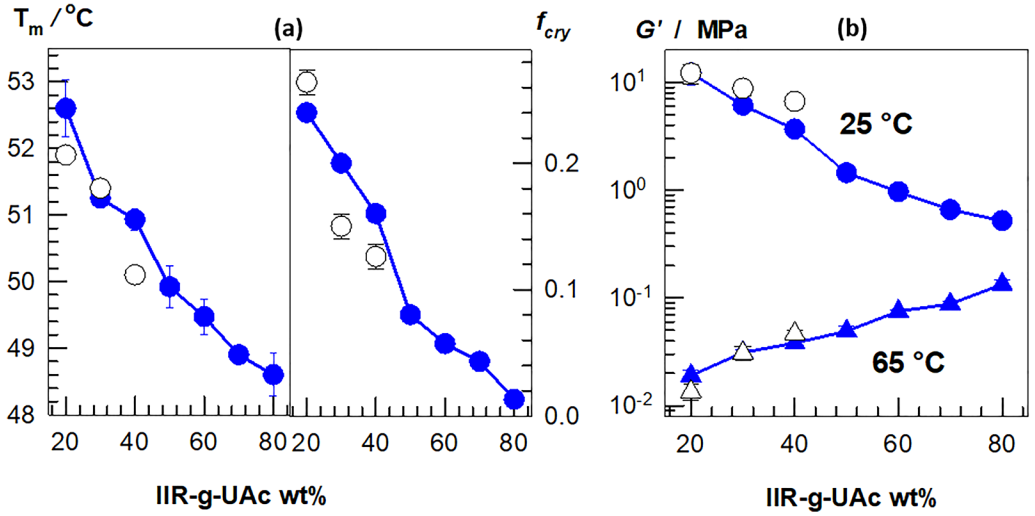

FIG. 9. (a) The melting temperature T_m, and the degree of crystallinity f_{cry} of IPNs formed in toluene plotted against the IIR-g-UAc content. (b) The storage modulus G' of the same IPNs measured at an angular frequency ω of 6.3 rad s^{-1} and at 25 and 65 °C. $\gamma_o = 1\%$. The open symbols in (a) and (b) represent the data of IPNs formed by bulk polymerization.

E. Effect of toluene diluent on IPN properties

Although solvent-free photopolymerization of C18A in the melt of grafted IIR is a simple and ecofriendly strategy to produce IPNs, the amount of the grafted rubber was limited at a maximum of 40 wt. % due to the high viscosity of the melt mixture. To further increase the rubber content of IPNs, toluene was included into the melt mixture, which is a good solvent for both components. We selected IIR-g-UAc as the grafted rubber for the preparation of IPNs in toluene as a diluent. The mixtures of the grafted rubber and C18A with 20–80 wt. % rubber content were dissolved in toluene at a fixed concentration of 59 wt. % and then subjected to the UV polymerization in the presence of Irgacure 2959 as described above. Figure 9(a) shows the melting temperature T_m and the degree of crystallinity f_{cry} of IPNs formed in toluene plotted against the IIR-g-UAc content. For comparison, the data of IPNs with IIR-g-UAc formed by bulk polymerization are presented by the open symbols. Both T_m and f_{cry} can be tuned between 49 and 53 °C and 1.3%–24%, respectively, by varying IIR-g-UAc content between 20 and 80 wt. % (Fig. S7 in the supplementary material [21]). Moreover, all IPNs formed in toluene exhibit temperature sensitivity in the modulus when the temperature is changed between below and above T_m, the extent of which decreases as the rubber content is increased [Fig. 9(b) and S8 in the supplementary material [21]]. At 25 °C, the storage modulus G' decreases with increasing rubber content due to the simultaneous decrease in the crystallinity while, at 65 °C, it increases with the rubber content due to the simultaneous increase of the viscosity of IPN in the molten state.

Figures 10(a) and 10(b) present tensile stress-strain curves and mechanical parameters of IPNs, respectively, containing 20–80 wt. % IIR-g-UAc. The dashed curves in (a) and open symbols in (b) represent the data of IPNs formed by bulk polymerization. It is seen that the brittle IPN turns into a highly stretchable one when the IIR-g-UAc content is

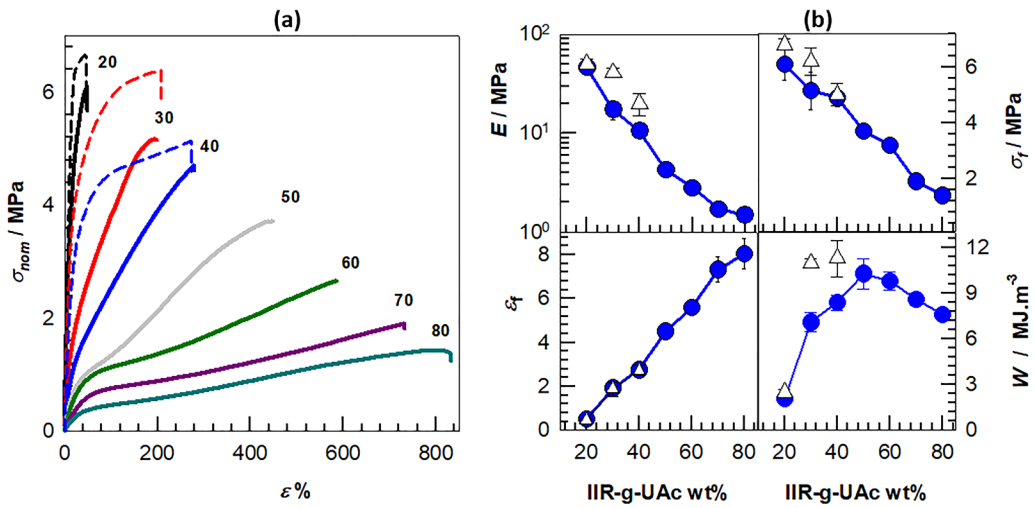

FIG. 10. The tensile stress-strain curves (a) and mechanical parameters (b) of IPNs formed in toluene with 20–80 wt. % IIR-g-UAc. The dashed curves in (a) and open symbols in (b) represent the data of IPNs formed by bulk polymerization.

increased from 20 to 80 wt. %. The mechanical parameters compiled in Fig. 10(b) reveal that they can be tuned over a wide range by changing the rubber content. For instance, the modulus decreases from 47 to 1.5 MPa while the elongation at break increases from 51% to 800% as the rubber content is increased from 20 to 80 wt. %.

As compared to IPNs formed by bulk polymerization, those formed in toluene exhibited a higher swelling ratio q_w and soluble fraction w_{sol} indicating decreasing chemical cross-link density $\nu_{e,chem}$ [Figs. S9(a) and S9(b) in the supplementary material [21]]. Calculations indeed reveal a decrease in $\nu_{e,chem}$ when comparing IPNs formed with and without toluene at the same rubber content, which is attributed to the intramolecular cross-linking reactions [Fig. S9(c) in the supplementary material [21]]. Similar to IPNs formed by bulk polymerization, those formed in toluene exhibited a self-healing efficiency of $93 \pm 4\%$ with respect to the modulus but a low efficiency with respect to the ultimate properties (Figs. S10 and S11 in the supplementary material [21]). They also exhibit shape-memory behavior with an efficiency decreasing as the rubber content is increased (Fig. S12 in the supplementary material [21]).

IV. CONCLUSIONS

Self-healing or self-recoverability is a promising approach emerged in the past decade to prolong the service life of polymeric materials and hence to reduce the load of waste polymers. Another important smart function, especially for biomedical applications, is shape-memory, a function that can memorize one or more shapes under the effect of a stimulus. Recently, a simple strategy was developed for preparing self-healing and shape-memory interconnected IPNs based on IIR and PC18A. Because IIR is soluble in C18A monomer, solvent-free UV polymerization of C18A in the presence of IIR results in IPNs with tunable thermal and mechanical properties together with self-healing and shape-memory functions. Here, we demonstrated that the use of IIR grafted with acrylic acid (IIR-g-AAc), methacrylic acid (IIR-g-MAAc), and 10-undecenoic acid (IIR-g-UAc) instead of unmodified IIR provides a significant improvement in the mechanical properties of IPNs. This improvement is due to vinyl groups pendant to IIR backbone increasing the extent of cross-linking between the IPN components. Calculations indeed show that IPNs exhibit around tenfold higher chemical cross-link density as compared to those formed from the native IIR. DSC measurements reveal a decrease in both T_m and T_{cry} by changing the type of the grafted monomers in the order of UAc > AAc > MAAc. The highest transition temperature reached using IIR-g-UAc is attributed to the long alkyl side chain of UAc stabilizing crystalline C18 side chains of PC18A. SAXS and WAXS measurements indeed demonstrate formation of the most stable alkyl crystals in IPNs when UAc is used as grafted monomer. TEM analysis reveals that the morphology of IPNs consists of an interconnected amorphous IPN matrix composed of noncrystalline PC18A and rubber components in which nano-sized crystalline domains are dispersed. IPNs exhibit up to a 3 orders of magnitude change in storage modulus when the temperature is changed between below and above their melting temperatures (46–52 °C). It was also found that the type of the grafted monomer significantly affects the mechanical properties. For instance, the highest modulus and fracture stress are obtained using AAc-functionalized IIR while MAAc functionalization produces the highest stretchability and toughness but relatively low modulus. The results can be explained with the relative contributions of chemical and physical cross-links to the total cross-link density of IPNs. All IPNs exhibit a complete self-recovery behavior induced by heating and an efficient shape-memory function. We also show that the amount of the grafted rubbers in IPN could be further increased up to 80 wt. % by the incorporation of toluene into the reaction system resulting in IPNs with a wide range of tunable thermal and mechanical properties.

ACKNOWLEDGMENTS

This work was supported by the Scientific and Technical Research Council of Turkey (TUBITAK), No. MAG-218M502. O.O. thanks the Turkish Academy of Sciences (TUBA) for the partial support.

AUTHOR DECLARATIONS

Conflict of interest

The authors declare that they do not have any financial or associative interest that represents a conflict of interest in connection with the work submitted.

REFERENCES

[1] Hager, M. D., S. van der Zwaag, and U. S. Schubert, *Self-Healing Materials*, Advances in Polymer Science Vol. 273 (Springer, New York, 2016).

[2] Creton, C., and O. Okay, *Self-Healing and Self-Recovering Hydrogels*, Advances in Polymer Science Vol. 285 (Springer, New York, 2020).

[3] Hernández Santana, M., M. den Brabander, S. García, and S. van der Zwaag, "Routes to make natural rubber heal: A review," Polym. Rev. **58**, 585–609 (2018).

[4] Behl, M., J. Zotzmann, and A. Lendlein, "Shape-memory polymers and shape-changing polymers," in *Shape-Memory Polymers and Shape-Changing Polymers*, Advances in Polymer Science Vol. 226, edited by A. Lendleini (Springer, New York, 2009), pp. 1–40.

[5] Su, E., C. Bilici, G. Bayazit, S. Ide, and O. Okay, "Solvent-free UV polymerization of n-octadecyl acrylate in butyl rubber: A simple way to produce tough and smart polymeric materials at ambient temperature," ACS Appl. Mater. Interfaces **13**, 21786–21799 (2021).

[6] Dakin, J. M., K. V. S. Shanmugam, C. Twigg, R. A. Whitney, and J. S. Parent, "Isobutylene-rich macromonomers: Dynamics and yields of peroxide-initiated crosslinking," J. Polym. Sci., Part A: Polym. Chem. **53**, 123–132 (2015).

[7] Xiao, S., J. S. Parent, R. A. Whitney, and L. K. Knight, "Synthesis and characterization of poly(isobutylene-co-isoprene)-derived macromonomers," J. Polym. Sci., Part A: Polym. Chem. **48**, 4691–4696 (2010).

[8] Cao, R., X. Zhao, X. Zhao, X. Wu, X. Li, and L. Zhang, "Bromination modification of butyl rubber and its structure, properties, and application," Ind. Eng. Chem. Res. **58**, 16645–16653 (2019).

[9] Okay, O., "Semicrystalline physical hydrogels with shape-memory and self-healing properties," J. Mater. Chem. B **7**, 1581–1596 (2019).

[10] Ebata, K., Y. Hashimoto, S. Yamamoto, M. Mitsuishi, S. Nagano, and J. Matsui, "Nanophase separation of poly(N-alkyl acrylamides): The dependence of the formation of lamellar structures on their alkyl side chains," Macromolecules **52**, 9773–9780 (2019).

[11] Osada, Y., and A. Matsuda, "Shape memory in hydrogels," Nature **376**, 219 (1995).

[12] Matsuda, A., J. Sato, H. Yasunaga, and Y. Osada, "Order-disorder transition of a hydrogel containing an n-alkyl acrylate," Macromolecules **27**, 7695–7698 (1994).

[13] Bilici, C., V. Can, U. Nöchel, M. Behl, A. Lendlein, and O. Okay, "Melt-processable shape-memory hydrogels with self-healing ability of high mechanical strength," Macromolecules **49**, 7442–7449 (2016).

[14] Lee, J. L., E. M. Pearce, and T. K. Kwei, "Morphological development in alkyl-substituted semiflexible polymers," Macromolecules **30**, 8233–8244 (1997).

[15] Bilici, C., and O. Okay, "Shape memory hydrogels via micellar copolymerization of acrylic acid and n-octadecyl acrylate in aqueous media," Macromolecules **46**, 3125–3131 (2013).

[16] Yang, Y., C. Wang, C. G. Wiener, J. Hao, S. Shatas, R. A. Weiss, and B. D. Vogt, "Tough stretchable physically-cross-linked electrospun hydrogel fiber mats," ACS Appl. Mater. Interfaces **8**, 22774–22779 (2016).

[17] Flory, P. J., *Principles of Polymer Chemistry* (Cornell University, Ithaca, NY, 1953).

[18] Durmaz, S., S. Fank, and O. Okay, "Swelling and mechanical properties of solution crosslinked poly(isobutylene) gels," Macromol. Chem. Phys. **203**, 663–672 (2002).

[19] Treloar, L. R. G., *The Physics of Rubber Elasticity* (University Press, Oxford, 1975).

[20] Mark, J. E., and B. Erman, *Rubberlike Elasticity* (Cambridge University, Cambridge, 2007).

[21] See supplementary material at https://www.scitation.org/doi/suppl/10.1122/8.0000414 for synthesis and characterization of the grafted rubbers, and details on the characterization of IPNs by solubility and swelling tests, their DSC, TEM, STEM, and mechanical test results.